



**HAL**  
open science

# Hydrodynamics and scale-up of bubble columns in the heterogeneous regime: Comparison of bubble size, gas holdup and liquid velocity measured in 4 bubble columns from 0.15 m to 3 m in diameter

Pedro Maximiano Raimundo, Ann Cloupet, Alain H. Cartellier, Davide Beneventi, Frédéric Augier

## ► To cite this version:

Pedro Maximiano Raimundo, Ann Cloupet, Alain H. Cartellier, Davide Beneventi, Frédéric Augier. Hydrodynamics and scale-up of bubble columns in the heterogeneous regime: Comparison of bubble size, gas holdup and liquid velocity measured in 4 bubble columns from 0.15 m to 3 m in diameter. *Chemical Engineering Science*, 2019, 198, pp.52-61. 10.1016/j.ces.2018.12.043 . hal-01999459

**HAL Id: hal-01999459**

**<https://hal.science/hal-01999459>**

Submitted on 31 Jan 2019

**HAL** is a multi-disciplinary open access archive for the deposit and dissemination of scientific research documents, whether they are published or not. The documents may come from teaching and research institutions in France or abroad, or from public or private research centers.

L'archive ouverte pluridisciplinaire **HAL**, est destinée au dépôt et à la diffusion de documents scientifiques de niveau recherche, publiés ou non, émanant des établissements d'enseignement et de recherche français ou étrangers, des laboratoires publics ou privés.

1  
2 **Hydrodynamics and scale-up of bubble columns in the heterogeneous regime:**  
3 **comparison of bubble size, gas holdup and liquid velocity measured**  
4 **in 4 bubble columns from 0.15m to 3m in diameter**

5  
6 *P. Maximiano Raimundo<sup>1,2</sup>, A. Cloupet<sup>1</sup>, A. Cartellier<sup>2</sup>, D. Beneventi<sup>3</sup>, F. Augier<sup>1,\*</sup>*

7  
8 *1- IFP Energies nouvelles, rond-point de l'échangeur de Solaize, 69360 Solaize*

9 *2- Université Grenoble Alpes, CNRS, Grenoble INP\*\* LEGI, F-38000 Grenoble, France,*

10 *3- Ecole Française de Papeterie et des Industries Graphiques, INPG, BP 65, F-38402 St. Martin d'Hères,*  
11 *France.*

12 \* Corresponding author, [frederic.augier@ifpen.fr](mailto:frederic.augier@ifpen.fr)

13 \*\* Institute of Engineering Univ. Grenoble Alpes

14  
15 **Keywords**

16 Bubble Column, Sauter Diameter, Scale-up, Velocimetry, Heterogeneous Regime, Experimental,  
17 Cross-correlation, Multiphase reactor, Clustering

18  
19 **Highlights**

- 20 • Bubble Sauter diameter, gas holdup and axial liquid velocity measurements are performed
- 21 • 0.15m, 0.4m, 1m and 3m diameter bubble columns are investigated
- 22 • A wide experimental database is furnished to assist further model developments
- 23 • Void fraction and liquid velocities profiles happen to be self-similar in the heterogeneous
- 24 regime
- 25 • The entrained liquid flow rate, proportional to  $D^{3/2}$ , is only set by the column diameter
- 26 • The quantity  $(gD)^{1/2}$  appears as a natural scale for mean and fluctuations velocities.

- 27 • Strong gas holdup gradients are present in the flow due to convective instabilities

28

## 29 **Abstract**

30 The development of CFD models coupled with Population Balance is a very promising topic  
31 concerning multiphase reactors. In the case of bubbly flows and bubble columns, a serious lack of  
32 local hydrodynamic characterizations still harms development and validation of relevant models. To  
33 fill partially this gap, a new bubble size measurement technique, previously introduced by Maximiano  
34 Raimundo et al. (2016), has been applied on a very wide range of bubble column diameters (from  
35 0.15m to 3m) and superficial gas velocities (from 0.06m/s to 0.35m/s). Size measurements have been  
36 coupled with others concerning gas holdup and axial liquid velocity, in order to provide an  
37 experimental database allowing to clarify the scale-up rules and to assist future modelling works.  
38 Average bubble sizes have been measured as globally similar at every scale. Measured holdup and  
39 average liquid velocity confirm already reported behaviours at lower column diameters. Liquid  
40 velocity fluctuations also follow self-similar radial profiles and are proportional to the average liquid  
41 velocity at the centre of the column leading to a strong turbulence intensity. The fact that the  
42 quantity  $(gD)^{1/2}$  appears as a natural velocity scale and the presence of strong gas-holdup gradients  
43 underline the similarity between bubble columns operated heterogeneous regime and free thermal  
44 convection in pipes.

## 45 **1. Introduction**

46

47 Although being a major research topic for decades, the design and scale-up of bubble column  
48 reactors is still a difficult task for chemical engineers, as associated hydrodynamic and transfer  
49 phenomena are very sensitive to physical properties of fluids, operating conditions and geometrical  
50 settings. A huge number of correlations have been developed in the past to assist scale-up by means  
51 of 0D or 1D approaches (Deckwer, 1992; Kantarci et al., 2005, Besagni et al., 2018). Available  
52 correlations are generally valid in rather narrow ranges of design parameters, physical properties and

53 operating conditions. Nowadays it is generally admitted that CFD can be used to secure industrial  
54 designs when outside of validation ranges of empirical correlations. But preliminary parameter  
55 adjustments are generally necessary to fit initial simulations on a given well investigated scale. The  
56 fitting step keeps CFD far from being a full predictive tool. Parameters to be adjusted can concern  
57 turbulence modelling, including Bubble Induced Turbulence (McClure et al., 2014 ; Joshi, 2001), but  
58 above all, interfacial forces (Jakobsen et al., 2005). There is no real consensus concerning the forces  
59 to consider to achieve realistic simulations, except for the drag law that all authors point out as  
60 impacting mostly the calculated gas holdup. The use of lift, added mass, wall lubrication and  
61 turbulent dispersion are sometimes suggested to improve the agreement between experimental  
62 data and CFD simulations (Krishna et al., 2001; McClure et al., 2015). However, during a previous  
63 work (Gemello et al., 2018b), it was found that time-averaged hydrodynamics (i.e. gas holdup and  
64 liquid velocity profiles) of several bubble columns were satisfactorily predicted using an apparent  
65 drag formulation as the only interfacial force. Nevertheless, the mean bubble diameter had to be  
66 beforehand known to perform such simulations, as it conditions directly the drag force, and thus gas  
67 holdup (Guedon et al., 2017). To overcome this limitation in presence of breakage and coalescence  
68 phenomena, one powerful possibility consists in associating CFD with a population balance on Bubble  
69 Size Distribution (BSD) (Buffo et al., 2013, Lehr et al., 2004, Sanya et al., 2005). If efficient, this would  
70 make CFD a much more predictive tool.

71 Whether to develop interfacial force models for CFD or Population Balance kernels, experimental  
72 data are essential, including information concerning bubble sizes in flow regimes of industrial  
73 interest. Only a few experimental data are usable for this purpose. Major of them are based on  
74 multitips optical probes (Chaumat et al., 2005, Xue, 2004, Xue et al., 2008, McClure et al., 2017).  
75 Multitips technique ideally allows to measure both bubble chord and velocity distributions. The  
76 technique is based on the processing of the phase-signal delay between probes located at different  
77 heights. As often pointed out by authors, its accuracy is acceptable at the centre of the column,  
78 where bubble have mostly vertical trajectories, but it rapidly decreases with the distance from it, as

79 bubble trajectories become more chaotic and include downward motion and the delay between  
80 signals is not linkable with the axial bubble velocity anymore. In addition, the performances of  
81 multitips probes in terms of minimum detectable bubble size are not clearly determined. An  
82 alternative approach consists in the use of a measurement technique independent of the bubble  
83 trajectory. This is the case of the cross correlation (CC) technique developed by Maximiano  
84 Raimundo et al. (2016) and validated in the heterogeneous regime by comparison with endoscopic  
85 measurements. The CC technique does not measure the global BSD, but only the mean Sauter  
86 diameter, i.e. the ratio between 3<sup>rd</sup> and 2<sup>nd</sup> moments of the BSD. But the measurements have the  
87 same accuracy regardless of the radial position. It has been applied recently to the study of the effect  
88 of water quality and the gas sparger design, in a 400mm column diameter (Gemello et al., 2018a).

89 In the present work, the same cross correlation technique has been used to measure bubble sizes in  
90 four bubbles columns from 0.15m to 3m in internal diameter, with the purpose of investigating the  
91 effect of scale-up on bubble sizes, for an identical gas/liquid system. Distilled or demineralized water  
92 are generally used in academic studies, but as tap water and air were the only fluids usable in the  
93 biggest column, a similar system has been used at all scales. The tap water used in the present work  
94 can be qualified as partially contaminated, as it exhibits a less coalescent behaviour than  
95 demineralized water. One limitation of using tap water is that its quality depends on the location and  
96 can lead to difficulties to repeat experiments elsewhere. To overcome this issue, It has been shown  
97 in (Gemello et al., 2018a) that the tap water used in the present study behaves as a solution of  
98 demineralized water containing 0.01% in weight of ethanol (Gemello et al., 2018a). In addition to the  
99 bubble size, the global ( $\langle\alpha_G\rangle$ ) and local ( $\alpha_G$ ) gas fractions have been measured via the liquid  
100 elevation measurement and the optical probes used for the cross correlation technique, respectively.

101 Axial liquid velocity profiles (average and fluctuation RMS values) have been also measured with a  
102 modified Pitot tube, so-called Pavlov tube technique (Forret et al., 2003). This technique is the only  
103 one usable at high gas holdup in all column sizes. Measurements have been done at different  $V_{sg}$   
104 from 0.03m/s to 0.35m/s depending on bubble columns. In the following, the four experimental

105 setups are introduced, as well as the involved measurement techniques. Then results concerning gas  
106 fraction, liquid velocity and bubble sizes are summarized and discussed. A discussion concerning the  
107 presence of bubble clusters and of voids (regions with few bubbles) and the role of these meso-scale  
108 structures on the hydrodynamics of the heterogeneous regime is finally proposed.

## 109 **2. Experimental setups**

110 In the present work, four different columns with 0.15 m, 0.4 m and 1 m and 3m inner diameters have  
111 been tested. All the experiments were conducted with compressed air, which had been dried and  
112 cooled, as the gas phase and with water, with no net liquid flow rate (batch mode), as the liquid  
113 phase. In the different columns, a partially contaminated tap water is used. Table 1 reports water  
114 analysis.

115 **Table 1: tap water analysis @ 20°C**

Surface tension (mN/m)	67
Conductivity @ 25°C ( $\mu\text{S}/\text{cm}$ )	559
Carbonate (mg/L)	$\approx 0$
Hydrogenocarbonate (mg/L)	251
pH	7.9

116  
117 In the four columns, the gas was introduced into the column from the base. The volumetric flow rate  
118 was determined by a row of several calibrated flow-meters, with an uncertainty given by suppliers  
119 equal to 1.6%. The gas distributors are perforated plates, the number of holes and their diameters in  
120 the different columns are given in the following table. The injectors have been designed to ensure  
121 comparable porosities (at a value small enough to uncouple the gas injection and the bubble column  
122 dynamics), and also to form gas jets with comparable ejection velocities (as the ejection velocity is  
123 equal to the superficial gas velocity divided by the porosity of the injection plates) which are  
124 expected to experience similar break-up process and thus to deliver comparable bubble size  
125 distributions at injection in all columns. Columns of 0.15 and 0.4m inner diameter exhibit exactly the  
126 same conditions of gas sparging with orifices 1mm in diameter and 10mm long. The injector for the  
127 1m inner diameter column has the same porosity, i.e. the same gas velocity at the outlet of injections

128 holes (from 13 to 140m/s), but the diameter of holes is doubled. Indeed, the effect of the hole size  
 129 can be considered as small as hole diameters stand much smaller than bubble sizes in the columns.  
 130 The biggest column is equipped with a different sparger, with larger and shorter injection holes and  
 131 with a lower porosity, but leading to comparable ejection gas velocities (from 37 to 100m/s).  
 132 However, Gemello et al. (2018a) have studied the impact of the sparger on the bubble size in the  
 133 0.4m inner diameter column used in the present study. It has been found that the sparger design has  
 134 an important effect at the bottom of the column. This effect is due both to the spatial gas  
 135 distribution, conditioned by the number of holes, and the bubble sizes generated by different  
 136 spargers, which can be very disparate. But the effect of the sparger becomes negligible above a  
 137 distance of 0.4m from the bottom of the column because of the dominant breakup phenomena  
 138 whatever the water quality. This behaviour is in agreement with the usual observation that, in the  
 139 heterogeneous regime, quantities such as local void fraction and velocities are weakly sensitive to  
 140 injection conditions when  $H_0/D > 2$  and when the data are gathered within the (almost) fully  
 141 developed region (Forret et al., 2006). In addition, it will be shown in section 4 that the mean bubble  
 142 sizes are similar for all columns and all flow conditions, probably thanks to an efficient break-up  
 143 process of the gas jets formed at injection.

144 **Table 2: gas distributors characteristics in the different columns**

Column	Number of holes	Hole diameter (mm)	Length/diameter ratio of injectors	Porosity (%)	Pitch (mm)
Ø0.15m	55	1	10	0.24	15 (triangular)
Ø0.4m	391	1	10	0.24	15 (triangular)
Ø1m	613	2	10	0.25	37 (triangular)
Ø3m	164	9	0.5	0.15	200 (squared)

145  
 146 The columns used in this study present of pairs of diametrically opposed holes at different heights  
 147 (0.5m, 1m, 1.5m, 2.6m, 3.4m and 4.6m above the gas distributor in the case of the 1 m in diameter  
 148 column), enabling the position of different technical means (Pavlov tube, optical probe...) or can be  
 149 used as pressure taps. The scheme of the 1 m in diameter column is given in the Figure 1. The  
 150 scheme of the other columns is very similar to this one.

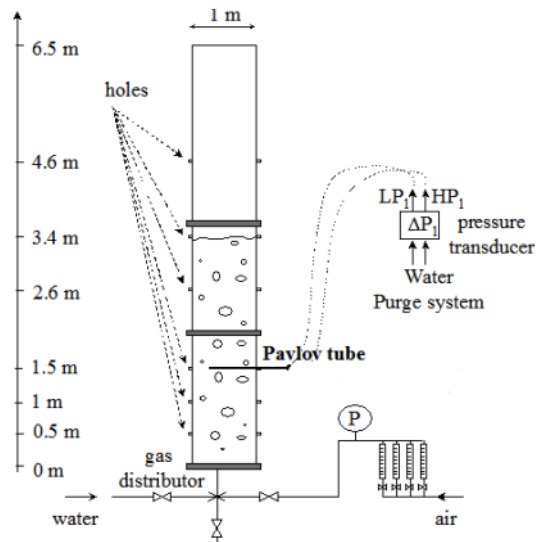


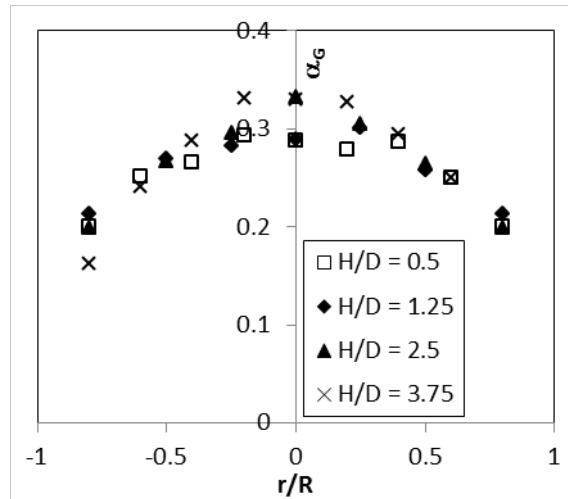
Figure 1: schematic view of the 1 m in diameter column and its perforated plate

151  
 152  
 153  
 154  
 155  
 156  
 157  
 158  
 159  
 160  
 161  
 162  
 163  
 164  
 165  
 166  
 167  
 168  
 169

In addition, the 0.15 m, 0.4 m and 1 m diameter columns were operated with a liquid static height/column diameter “aspect ratio” ( $H_0/D$ ) of 4. The 3 m diameter column has operated with 2.2 liquid static height/diameter ratio because the column is only 12 m high. Besagni et al. (2017a) studied the effect of the aspect ratio on the gas holdup and suggested a critical aspect ratio of 5. Nevertheless, exhaustive experimental results reported by these authors show that above 3-4, the effect of the aspect ratio on gas holdup becomes very weak. This is also confirmed by the measurements of Sasaki et al. (2016). Measurements have been performed at an elevation height of 2.5 times the column diameter ( $H/D=2.5$ ), except in the 3m column, inside which measurements are performed at  $H/D=2$ . According to Forret et al. (2006), such elevations are indeed within the fully developed flow region. However, the recent work of Guan et al. (2016) may lead to moderate this conclusion. They found that gas holdup and liquid velocity radial profiles were never totally independent of the axial position in a column of 0.8m in diameter. Yet, using a uniform gas sparger, the flow happens to be almost fully developed between  $H/D$  from 2 to 4. Guan et al. (2016) also suggested that the height of flow development depends on the column diameter. Figure 2 reports gas holdup profiles measured in the  $\varnothing 0.4\text{m}$  column at  $V_{sg}=0.16\text{m/s}$  and at different heights. Profiles measured at  $H/D = 2.5$  and 3.75 are similar, while some discrepancies are observed below, especially

170 in the middle of the column. In summary, the aspect ratio of the studied columns is considered to be  
 171 sufficient to neglect its effect on hydrodynamics, and the height of measurement is comprised within  
 172 the range of fully developed flow.

173



174

175 **Figure 2 : Comparison of gas holdup profiles measured in the Ø0.4m column at different H/D. V<sub>sg</sub>=0.15m/s (H<sub>0</sub>/D=4)**  
 176

177

### 178 3. Measurement techniques

#### 179 3.1. Gas holdup

180 The global gas holdup can be directly calculated by the visual observation of the expansion of liquid  
 181 height by:

182

$$183 \langle \alpha_G \rangle = 1 - \frac{H_0}{H_D} \quad (1)$$

184

185 Where  $\langle \alpha_G \rangle$  represents the global void fraction,  $H_0$  represents the non-aerated liquid height and  $H_D$   
 186 the aerated liquid height. In the present study, the liquid height is measured by visual observation  
 187 along a graduated rule, and fluctuations of liquid level induce a relatively high uncertainty of the

188 measurement, estimated at 10%. Sasaki et al. (2016) strongly decreased the uncertainty while using  
189 image processing to detect liquid level. The local gas holdup was measured by a light reflective  
190 optical probe. The beam is generated by a laser and is sent through the optical fiber to the point of  
191 the probe. If the probe is in contact with the liquid phase, the light beam is refracted through the  
192 liquid media. Otherwise, if the probe tip is in contact with the gas phase, the light beam is reflected  
193 by the bubble into the probe tip and then detected by a photodiode where the light beam intensity is  
194 converted into voltage. Adding the time that the probe detects the gas phase, the local gas hold up is  
195 determined by the following equation.

196

$$197 \quad \alpha_G = \frac{\text{Cumulated gas time}}{\text{Experimental time}} \quad (2)$$

198

199 The local gas holdup detected with the optical probe was compared with global gas hold-up for  
200 heterogeneous conditions in the 0.4m bubble column. The agreement was within  $\pm 15\%$  (Maximiano  
201 Raimundo et al., 2016), which is satisfactory owing to the uncertainty on the determination of  $\langle \alpha_G \rangle$ .

202

### 203 3.2. Cross-Correlation (Bubble size)

204 In order to characterize bubbles in dense, heterogeneous bubbly flows such as those encountered in  
205 industrial bubble columns, a recently developed measuring technique based on the spatial  
206 correlation of phase indicator functions is proposed (Maximiano Raimundo et al., 2016). The  
207 normalized cross-correlation is a function that quantifies the similarity of two binary signals by  
208 analysing both signals simultaneously:

$$209 \quad CC = \frac{\int_{t=0}^{t^{exp}} \text{Signal}_A(t) \times \text{Signal}_B(t) dt}{\int_{t=0}^{t^{exp}} \text{Signal}_A(t) dt} \quad (3)$$

210

211 Here  $Signal_A$  and  $Signal_B$  represent the raw signals coming from two different probes at the same  
 212 elevation in the column at a radial distance ( $d$ ) and  $t_{exp}$  represents the time of registration. The  
 213 cross-correlation value is maximal if both probes are at the same point in space (distance between  
 214 probes  $d$  of 0 mm), since the signals will be identical. In a single bubble-probe interaction, as the  
 215 distance between the probes increases, the cross-correlation of the probe signals will decrease. The  
 216 cross-correlation will be zero when the distance between probes becomes larger than the bubble  
 217 horizontal diameter due to the fact that the same bubble cannot be detected by both probes at the  
 218 same time. Nevertheless, in a bubble column, the cross-correlation is never zero even if the distance  
 219 between probes reaches a value much larger than the largest bubble horizontal diameter. At large  
 220 distances, the cross-correlation tends to the local gas hold-up  $\alpha_G$ . It has been shown that some  
 221 information related to the horizontal bubble size can be extracted from the initial linear slope of the  
 222 cross-correlation curve as a function of probes distances (Maximiano Raimundo et al., 2016). The  
 223 relationship between the Sauter mean value of horizontal bubble diameters, noted  $d_{32,h}$ , the  
 224 correlation coefficient CC and the inter-probes distance  $d$  always expresses as follows:

$$226 \quad d_{32,h} = a \frac{d}{(CC(d)-1)} \quad (4)$$

227  
 228 where the prefactor  $a$  is function of the bubble shape, as detailed in the following table (details in  
 229 Maximiano Raimundo et al., 2016).

231 **Table 3: Prefactors  $a$  for various bubble shapes**

	Sphere	Oblate	Prolate with Ecc=0,7
Prefactor a	-1.472	-1.5978	-1.7

232  
 233 To validate this method, it has been compared to endoscopic imaging. The Sauter mean horizontal  
 234 diameters detected with the correlation technique happen to be in good agreement with those  
 235 provided by endoscopic imaging. This latest method enables also the determination of the average

236 eccentricity ( $ecc$ ) : the latter has been measured equal to 0.7 for all flow conditions and all column  
 237 dimensions except for the 3m I.D. column for which the eccentricity was not measured. Therefore,  
 238 the Sauter mean diameter  $d_{32}$  can be linked to the  $d_{32,h}$  measured by the cross-correlation as follows.

239

$$240 \quad d_{32} = d_{32,h} * ecc^{1/3} \quad (5)$$

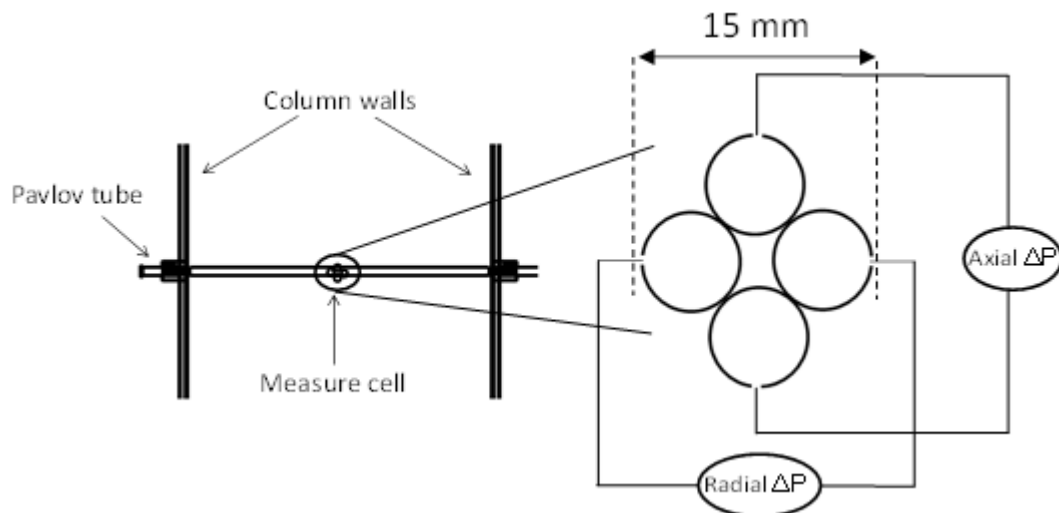
241

242 with  $ecc = 0.7$ .

243

### 244 3.3. Pavlov tube(axial liquid velocity)

245 The Pavlov tube used in this work is composed by four 5 mm diameter tubes, arranged as it is shown  
 246 in the right-hand side of the Figure 3. The four tubes are placed inside a 30 mm diameter tube, which  
 247 crosses horizontally the column, in order to obtain rigidity and to allow horizontal displacement. The  
 248 5 mm diameter tubes are completely closed, except for a 0.5 mm diameter lateral hole that assures  
 249 that the pressure inside the tube is equal to the one in the column.



250

251 **Figure 3: Schematic representation of the Pavlov tube (Axial measurements are performed along a vertical axis, radial**  
 252 **measurements are performed along a horizontal axis)**

253

254 The holes of the tubes on the vertical plan are placed in the same axis but in opposite  
 255 directions, as depicted in Figure 3. Additionally, each tube on the vertical direction is connected to

256 one of the chambers of a differential pressure sensor. These tubes serve to measure the axial  
257 pressure difference, since the holes on the tubes are aligned with the column vertical axis. The  
258 Pavlov tube allows also the measurement of the radial liquid velocity, quite low in this study, not  
259 discussed in this paper. The measurements of the axial pressure differences ( $\Delta P$ ) can be used to  
260 calculate the instantaneous axial liquid velocity recurring to the following equation.

$$261 \quad U_{(x,t)} = \begin{cases} \sqrt{\frac{2\Delta P(x,t)}{\rho_l}} & \text{if } \Delta P(x,t) \geq 0 \\ -\sqrt{\frac{-2\Delta P(x,t)}{\rho_l}} & \text{if } \Delta P(x,t) < 0 \end{cases} \quad (6)$$

262 The axial  $\Delta P$  measurement was made with a differential pressure transmitter Rosemount 3051T with  
263 a range of  $\pm 60$  mbar, a frequency of 8 Hz and resolution of 0.01 mbar. Let us mention that corrections  
264 of eq.(6) accounting for local void fraction have been sometimes proposed. On one hand, the largest  
265 of these corrections is the one proposed by Bosio and Malnes as discussed by Riemann et al. (1984).  
266 According to that correction, the difference in velocity prediction remains smaller than 3% since  
267 the void fraction are always below 35% in all our experiments. On another hand, these corrections  
268 consider that the dynamic pressure collected from pitot or pavlov tubes in two-phase flows is  
269 associated with the density and the velocity of the mixture. However, in bubbly flows, the orifices of  
270 pitot or pavlov tubes are always wetted, meaning that the gas phase is never detected as such.  
271 Therefore, the local stopping pressure detected with such sensors provides a measure of the local  
272 liquid velocity even when the sensor is in the vicinity of a bubble, and no correction is required. All  
273 Pavlov tube measurements presented hereafter are grounded on eq.(6).

274 The radial profiles are easily obtained by moving the measuring cell along the column radius. The  
275 axial velocity fluctuations can be calculated through the instantaneous and the averaged velocity,  
276 using Reynolds decomposition, as presented in the following equation.

277

$$278 \quad U(x,t) = U(x) + u'(x,t) \quad (7)$$

279

280 where  $U(x)$  represents the mean liquid velocity,  $u'(x,t)$  represents the liquid fluctuation velocity  
281 at the instant  $t$  and  $U(x,t)$  represents the liquid velocity at the instant  $t$ .

282

#### 283 **4. Results**

284 Thereafter, the discussion focuses on the heterogeneous regime. On all columns, one can observe in  
285 Figure 4, that the almost linear behaviour of  $\langle\alpha_G\rangle$  with  $V_{sg}$  is observed only below 4-5cm/s,  
286 approximately. This value corresponds to the transition to the heterogeneous regime.

##### 287 *4.1. Gas holdup*

288 Global gas volume fractions have been measured for all columns and  $V_{sg}$ . Radial gas holdup profiles  
289 have been measured with the optical probes at  $H/D=2.5$  (Figure 4). Schweitzer et al. (2001) found  
290 similar profiles of  $\alpha_G(x)$  when normalized by the average gas holdup in the column  $\langle\alpha_G\rangle$ . Authors  
291 suggest the correlation reported in eq.(8) to represent holdup profiles. The correlation has been  
292 initially developed and validated in a 50mm inner diameter column for  $V_{sg}$  between 0.03 to 0.25m/s.  
293 Its range of validity has been extended by Forret et al. (2006) to columns up to 1m of inner diameter.

294

$$295 \alpha_G(x) = \langle\alpha_G\rangle[-1.638(x^6 - 1) + 1.228(x^4 - 1) - 0.939(x^2 - 1)] \quad (8)$$

296

297 On Figure 4 (left), unsurprisingly it is verified that gas holdup follows the same profile at any scale,  
298 with an average error below 5%. Concerning the average gas holdup, keeping in mind that the liquid  
299 elevation measurement method eq.(1) is relatively imprecise (+/- 10%), different correlations  
300 validated in air/water systems may be found in acceptable agreement with present experimental  
301 data. As the gas holdups have been measured with the same technique and using the same water,  
302 experimental data have been used to fit a new correlation in the aim to extract the specific effect of  
303 scale up in the heterogeneous regime. Remember that existing models have been generally

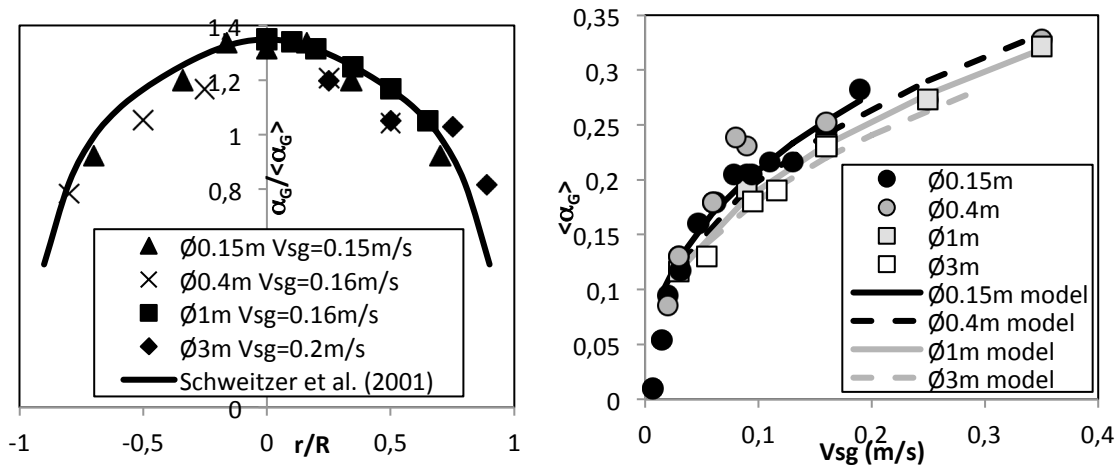
304 developed based on a single column diameter, generally lower than 0.4m. The following correlation  
 305 has be found to predict  $\langle \alpha_G \rangle$  with an error below 6% when  $V_{sg} > 0.1\text{m/s}$ :

306

$$307 \quad \langle \alpha_G \rangle = 0.49 \cdot V_{sg}^{0.41} \cdot D^{-0.047} \quad (9)$$

308

309 Measured and predicted average gas holdups are compared in Figure 4 (right). Only experiments  
 310 corresponding to  $V_{sg} > 0.05 \text{ m/s}$  are considered to fit eq.(9), given that gas holdup is proportional to  
 311  $V_{sg}$  in the homogeneous regime. It is observed a small, but not negligible effect of the column  
 312 diameter on the gas holdup, especially in intermediate range of  $V_{sg}$ , between 0.1 and 0.2 m/s.  
 313 Although most of existing correlations do not include the effect of  $D$  (Kantarci et al., 2005), the  
 314 question of the impact of the column diameter on the gas holdup is still not completely settled as  
 315 notably discussed by Rollbush et al. (2015). Additional experiments may although be necessary at  
 316 higher  $D$  to confirm this trend, as at high  $V_{sg}$  measurements in 0.4 and 1m diameters are relatively  
 317 close. Alternatively the eq. (9) can be replaced by an equation involving only  $V_{sg}$  with an exponent of  
 318 0.41 and a prefactor of 0.5 instead of 0.49, with a mean error of 8%.



319

320 **Figure 4: Gas holdup profiles at  $H/D=2.5$ , normalized by the average gas holdup (left), and average gas holdup**  
 321 **measurements (right). Comparison with correlations (eq. 8&9).**

322

323 4.2. Liquid velocity

324 In a similar manner, Forret et al. (2006) suggested to normalize axial liquid average velocity profiles  
325 by the liquid velocity at the center  $U_0$ , and found a good agreement with the following polynomial  
326 model:

327

$$328 \quad U(x) = \frac{U_0}{a-c} [a \cdot \exp(-b \cdot x^2) - c] \quad (10)$$

329

330 With  $a=2.976$ ,  $b=0.943$ ,  $c=1.848$ . The eq. (10) has been compared to the present experimental  
331 measurements of  $U(x)$ , and a very good agreement has been found, except in the largest column  
332 where the magnitude of the liquid velocity close to the walls is slightly underestimated by the model.  
333 The comparison between  $U(x)/U_0$  and eq.(10) are reported in Figure 5. The liquid velocity at the  
334 center can also be correlated with  $V_{sg}$  and  $D$ . The equation (11) presents the result of the regression,  
335 which predicts  $U_0$  with an average error below 8%:

336

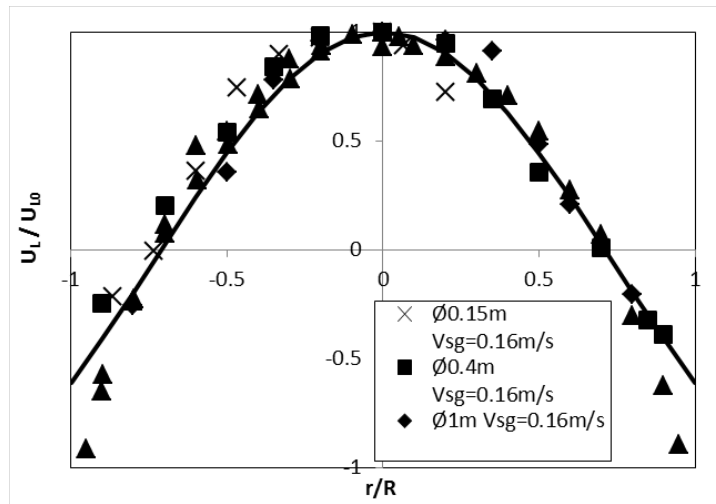
$$337 \quad U_0 = 1.35 \cdot V_{sg}^{0.16} \cdot D^{0.40} \quad (11)$$

338

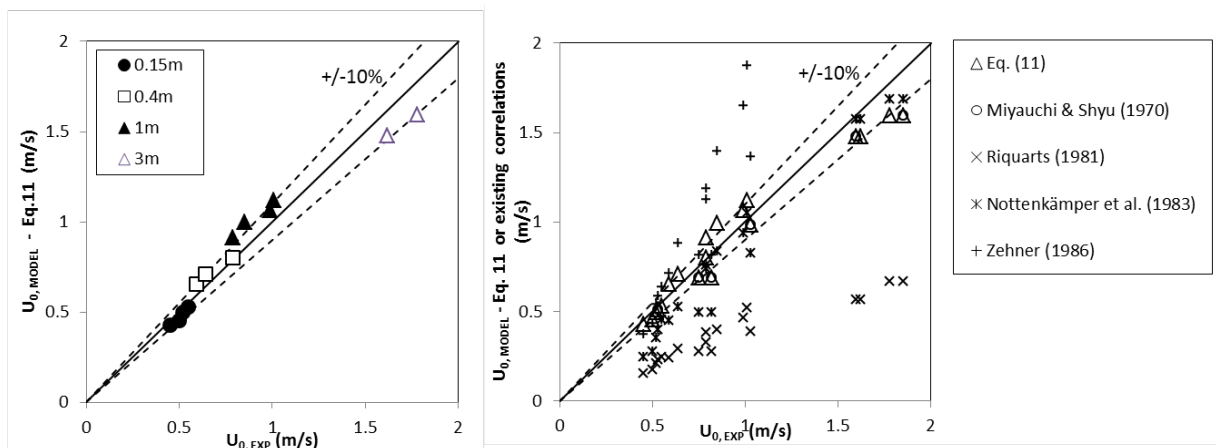
339 Figure 6 (left) presents the parity diagram between eq.(11) and experimental measurements in  
340 different columns. In Figure 6 (right), experimental results are also compared to a short selection of  
341 existing correlations of Miyauchi & Shyu (1970), Riquarts (1981), Nottenkämper (1983) and Zehner  
342 (1986). In this figure, each experimental centreline velocity, reported in abscissa, is compared to the  
343 velocity given by the different listed correlations, including eq.11, at the same operating  $V_{sg}$  and  $D$ ,  
344 which are reported in ordinate. This comparison shows that our experiments are in good agreement  
345 with previous works of Miyauchi & Shyu (1970) and Nottenkämper (1983), but not with others,  
346 pointing out the disparity of experimental results obtained in different laboratories. This disparity can  
347 have different origins, as the different measurement methods, different quality of water, different

348 gas sparging conditions or different column sizes. The present study allows to eliminate the 3 first  
 349 possibilities.

350 While the exponent on D in eq. (11) is quite classical – in the range of 0.3-0.7, the exponent on Vsg  
 351 can be considered lower than generally observed (0.3-0.5). This later result may be a consequence of  
 352 the quality of water, which partially prevents coalescence when compared with non-contaminated  
 353 water, resulting in a less pronounced heterogeneity of bubble sizes and possibly a lower liquid  
 354 recirculation as suggested by Rollbusch et al. (2015). Thus, from the above results, it happens that  
 355 the flows in bubble column operated in the heterogeneous regime self-organise, leading to self-  
 356 similar radial profiles for the void fraction and for the mean liquid velocities.



357  
 358 **Figure 5: Normalized liquid velocity profiles (left) and comparison between the axial average liquid velocity at the center**  
 359  **$U_0$  and eq.(11).**



360  
 361  
 362 **Figure 6: Centre-line velocity parity diagram of eq.11 (left) ; parity diagram of different correlations (right)**

363

364

365 Besides, a well-known behaviour concerning the liquid velocity profile is observed: the section of the  
366 columns can be divided into two surfaces of equal area: the core region when  $r < \frac{\sqrt{2}}{4}D$  or  $x < 0.71$ , where  
367  $U$  is positive, and the external region where  $U$  is negative. In the core region, the liquid upward flux  
368 can be calculated as:

369

$$370 \quad Q_{L,up} = \int_0^{\frac{\sqrt{2}}{4}D} 2\pi \cdot r \cdot (1 - \alpha_G) \cdot U(r) \cdot dr \quad (12)$$

371

372 The calculated liquid upward flux for three  $V_{sg}$  and for all the investigated columns are reported in  
373 Figure . The liquid upward flux surprisingly happens to be independent of the superficial gas velocity  
374 in the heterogeneous regime. Results correlates very well with  $\propto D^{2.5}$ , implying that the average  
375 liquid velocity in the core region follows a trend  $\propto \sqrt{D}$ . One possible explanation of that could be the  
376 predominant role of the natural velocity scale  $\sqrt{gD}$ . If we define a Froude number based on the  
377 mean liquid velocity in the core region of section  $S_{core} (= \pi D^2/8)$ , a constant value of the Froude  
378 number is observed:

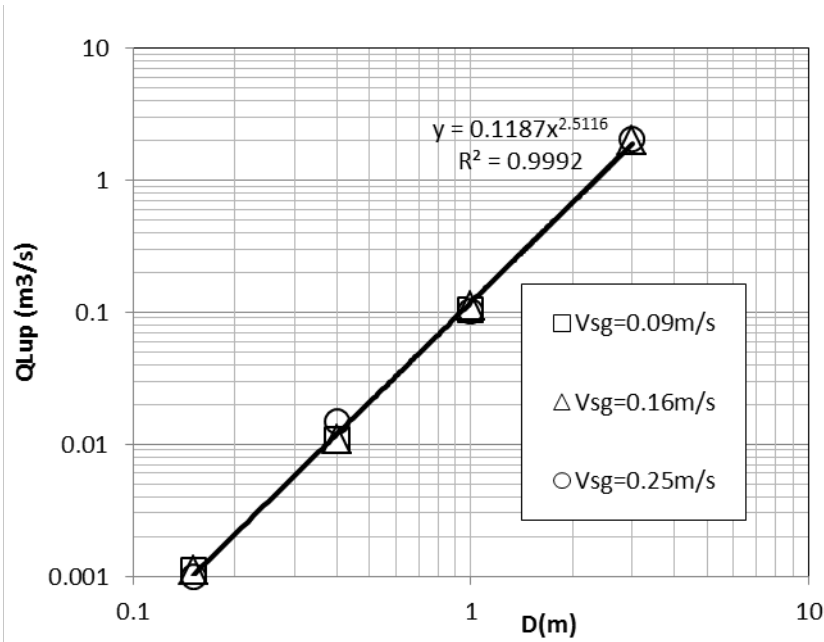
379

$$380 \quad Fr = \frac{Q_{L,up}}{S_{core}\sqrt{gD}} \approx 0.024 \quad (13)$$

381

382 This result also illustrates the close link between liquid volume fraction and velocity profiles, as both  
383 change with the gas flow rate but not their mutual product. The above velocity scaling and the  
384 observed flow organisation are reminiscent of free thermal convection in pipes for which the natural  
385 scale for velocity has been shown to be the free fall velocity under buoyancy acceleration evaluated  
386 for a length scale equal to the pipe diameter (Tisserand et al., 2010, Rusaouen et al., 2014).

387



388

389 **Figure 7: Liquid upward flux in the core region as a function of the bubble column diameter for the heterogeneous**  
 390 **regime.**

391

392 *Relative velocity*

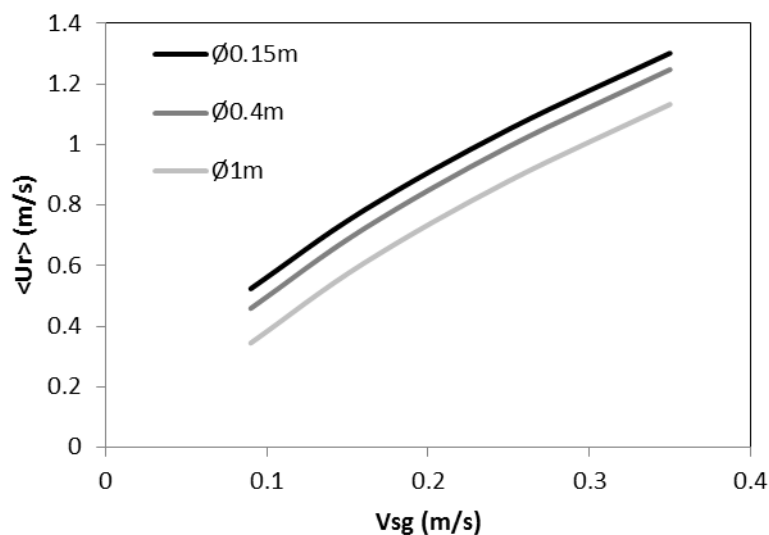
393 In the core region, the mean flow is directed upward and it is thus similar to a co-current upward  
 394 two-phase flow. According to classical kinematic approaches (e.g. Zuber and Findlay 1965), the  
 395 difference between the gas flow rate fraction defined as the volumetric gas flow divided by the sum  
 396 of liquid and gas volumetric flow rates and the void fraction is controlled by the relative velocity  
 397 between phases. In the same spirit, let us introduce the apparent (in the sense that it is a global  
 398 quantity at the scale of the core region of the column and not a local one) relative velocity between  
 399 gas and liquid  $\langle Ur \rangle$  in the core region as the difference of mean velocities between gas and liquid in  
 400 the core section. Each mean velocity is calculated as the phasic volumetric flow rate divided by the  
 401 associated cross section, i.e. the core section multiplied by the volume fraction of the concerned  
 402 phase in this section:

403

$$404 \langle Ur \rangle = \frac{Q_{G,core}}{\langle \alpha_G \rangle_{core} \cdot S_{core}} - \frac{Q_{L,up}}{(1 - \langle \alpha_G \rangle_{core}) \cdot S_{core}} \quad (14)$$

405

406 Where  $Q_{G,core}$  is the gas flow rate in the core region,  $Q_{L,core}$  the liquid flow rate in the core region is  
 407 given by (eq.(13) and  $\langle\alpha_G\rangle_{core}$  is computed from eq. (8) and is found  $\approx 1.33 \langle\alpha_G\rangle$ .  $Q_{G,core}$  can be  
 408 roughly estimated by the total gas flow rate  $Q_G$ . Note that this approximation tends to minimize the  
 409 estimation of the relative velocity as the recirculation of a part of the bubbles is not taken into  
 410 account. The estimation of relative velocities are reported in Figure 8 for  $V_{sg} > 0.09\text{m/s}$  and for three  
 411 columns. The relative velocity increases with  $V_{sg}$  and achieves values that are much higher than the  
 412 terminal bubble velocity ( $\approx 0.22\text{m/s}$ ). Such an increase in the bubble relative velocity in the  
 413 heterogeneous regime has been evoked by Ruzicka (2013). Possible origin of this phenomenon is  
 414 discussed below.



415  
 416 **Figure 8: Estimation of the relative velocity in the core region, considering that the gas flow rate in the core region equals**  
 417 **the totality ( $Ur_{max}$ ) or the half ( $Ur_{min}$ ) of the total gas flow rate.**

418  
 419 *Fluctuating velocity*

420 RMS of axial liquid velocity fluctuations ( $u'$ ) have been measured in various operating conditions.  
 421 Results presented in Figure 9 (left) point out that  $u'$  radial profiles also follow self-similar profiles. The  
 422 following polynomial function has been regressed in eq. (15) and is also reported in Figure 9 (left) to  
 423 illustrate the self-similarity of profiles.

424

425  $u'(x) = u'(0.71) \cdot [a + bx^2 + cx^4 + dx^6]$  (15)

426

427 With  $a=0.48$ ,  $b=2.25$ ,  $c=-2.6$ ,  $d=0.40$ . The normalization of the  $u'$  profiles can be done whatever the  
 428 position of reference ( $x$ ) but it has been found that using the maximal  $u'$  value minimizes the error of  
 429 residues of the regression. The maximal value of  $u'$  is always located at the boundary between  
 430 positive and negative liquid velocities ( $x = \sqrt{2}/2 \approx 0.71$ ). When comparing  $u'_{max}$  at different scales, it  
 431 is found proportional to  $U_0$ . As a consequence, the maximal  $u'$  value can be written as follows:

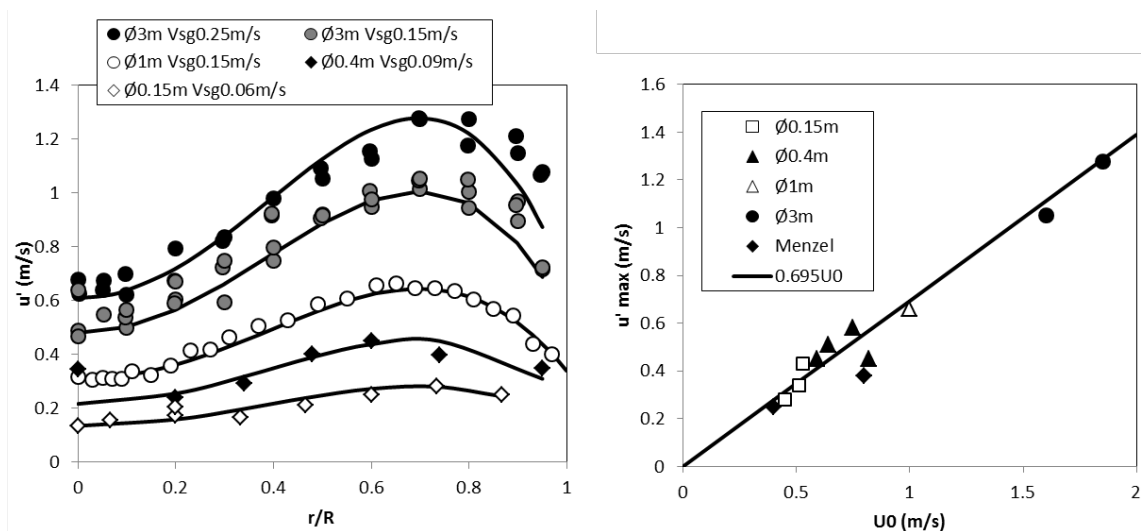
432

433  $u'(x = \sqrt{2}/2) = u'_{max} = 0.695 U_0$  (16)

434

435  $u'_{max}$  is reported in Figure 9 (right) for the different columns. The experimental data of Menzel et al.  
 436 (1990) using a hot wire probe is also reported on the same figure. The consistency between the  
 437 values measured with different techniques confirms the reliability of Pavlov tube measurements  
 438 concerning axial liquid velocity fluctuations. Note that in the core region, the liquid fluctuations are  
 439 about half their maximum, corresponding to a turbulent intensity  $u'/U_0$  about 25-30%. Hence, large  
 440 velocity fluctuations are present over the entire cross-section at all flow conditions: that feature is a  
 441 clear characteristic of the heterogeneous regime.

442



443

444 **Figure 9:  $u'$  radial profiles (left) and correlation between  $u'(x=0,71)$  and  $U_0$  (right).**

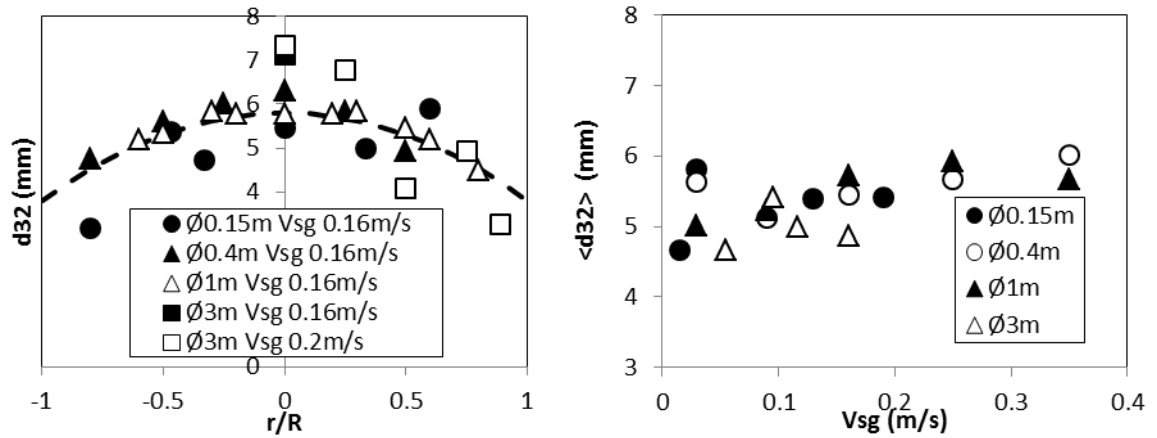
445

#### 446 *4.3. Bubble diameters*

447 Sauter mean diameters measured with the cross-correlation technique are reported in Figure 10. On  
448 the left, bubble Sauter diameter ( $d_{32}$ ) profiles are reported at a given  $V_{sg}$ . On the right, volume  
449 average Sauter diameters  $\langle d_{32} \rangle$  for the 4 columns are given as a function of  $V_{sg}$ .  $\langle d_{32} \rangle$  is computed  
450 as the gas-volume averaged Sauter diameter over column sections. Let us recall that, in the up-flow  
451 region, the typical relative uncertainty on the Sauter diameter is less than 10% for the large  
452 superficial velocities considered here (Maximiano Raimundo et al., 2016). Important results can be  
453 summarized as follows:

- 454 • The mean bubble diameter increases slowly from  $\approx 4.5 - 5$  mm at low  $V_{sg}$  to 5.5-6mm at high  
455  $V_{sg}$
- 456 • The mean bubble diameter is almost insensitive to the column diameter,
- 457 • Bubble size profiles follow roughly a parabolic shape, as suggested by the parabolic function  
458  $(y=5.8-2x^2)$  reported in Figure 10.
- 459 • Bigger bubbles are measured at the center of the column, and the bubble size decreases with  
460  $x$  typically by 1 to 2mm indicating that a small amount of spatial segregation between upflow  
461 and downflow regions occurs in these flows.

462 In all our experiments, the terminal velocity of the average bubbles varies over a limited range (0.21-  
463 0.23m/s in clean water), and the bubbles always pertain to the same regime i.e. ellipsoids at high  
464 particulate Reynolds number (the latter ranges between 950 and 1300) experiencing wobbling (Clift  
465 et al., 1978). Hence, the present database has been built-up for nearly the same mean bubble size  
466 irrespective of the dimension of the bubble column and of the amount of gas injected.



467

468 **Figure 10: Sauter diameter profiles in the 4 columns (right) and volume average Sauter diameter for the 4 columns versus**  
 469  **$V_{sg}$ . ( $H/D=2.5$  except in the 3m column where  $H/D=2$ ).**

470

471 As the mean bubble size does not exhibit strong variations for  $V_{sg}$  in the range of 0.03 to 0.35 m/s,  
 472 this quantity does not explain by itself the transition between the homogeneous and the  
 473 heterogeneous regime. Further investigation based on bubble size distributions may be required to  
 474 identify a presumed link between coalescence phenomena and flow regime transition as suggested  
 475 and reviewed by Besagni and Inzoli (2017b).

476

#### 477 4.4. Discussion

478 Bubble size measurements suggest information concerning turbulence. Classical population balance  
 479 kernels (Buffo et al., 2013) use the dissipation rate ( $\varepsilon$ ) as a major parameter to predict breakage and  
 480 coalescence.  $\varepsilon$  can classically be written as  $\sim u'^3/\Lambda$ ,  $\Lambda$  being a turbulence macroscale. Besides, the  
 481 global dissipation rate inside bubble columns can be estimated via different ways, but it is generally  
 482 considered as not depending on the column diameter (Deckwer, 1992; Roels and Heijnen, 1980).  
 483 Indeed in bubble columns  $\varepsilon$  is usually calculated as  $g \cdot (\rho_L - \rho_G) / \rho_L \cdot V_{sg}$ . The observed almost  
 484 constant bubble size with scale-up is consistent with this theory. In the present study  $u'$  has been  
 485 found to follow  $\sim D^{0.4}$ , this implies that  $\Lambda$  increases during scale up as  $\sim D^{1.2}$ , let say  $\sim D$ , which makes  
 486 sense from a pure geometrical consideration. Further investigations concerning the size of  
 487 turbulence macroscales in bubble columns may be useful to understand the link between flow

488 structures and turbulence production, as well as with breakage and coalescence phenomena.

489 Concerning velocity scales, the above discussion on the apparent relative velocity indicates that the

490 terminal velocity of bubbles is not the most relevant scale in these buoyancy driven bubbly flows.

491 Indeed, a natural velocity scale  $(gD)^{0.5}$  arises from the analysis of the entrained liquid flow rate in the

492 central portion of the column. Such a scale is reminiscent of turbulent flows driven by convection. In

493 buoyancy driven flows such as in thermal convection, the equilibrium between flow convection and

494 Archimedian forcing leads to a velocity scaling as  $V^2 \approx gL\Delta\rho/\rho$ , where the density gradient  $\Delta\rho$  is

495 evaluated at the length scale  $L$ .  $L$  is tentatively taken here as the column diameter. That choice is

496 supported here by the fact that we are considering the fully developed region, and, as the flow

497 happens to be self-similar in that zone, the height of the column is no longer a relevant parameter.

498 In addition to these large-scale gradients, localised variations in the density of the gas-liquid mixture,

499 equivalent then to variations in the local gas concentration, can also arise. Indeed, dispersed two-

500 phase flows can be prone to the formation of clusters, and Voronoï tessellations that are an efficient

501 way to detect and characterise such clusters (Monchaux et al., 2012) have been exploited here.

502 In the present experiments, we exploited the signals delivered by optical probes that provide the

503 arrival time of bubbles. From such a time history, it is straightforward to define successive Voronoï

504 time intervals  $\Delta T_{\text{bubble}}$  containing a single bubble centred into it. Figure 11 provides the statistics

505 gathered on the axis of the 1m I.D. column at  $V_{\text{sg}} = 25\text{cm/s}$ : the data correspond to a record of 600

506 seconds during which 85000 bubbles have been detected. The abscissa in Figure 11 is the time

507 interval  $\Delta T_{\text{bubble}}$  normalised by the mean value  $\langle \Delta T_{\text{bubble}} \rangle$ . The quantity  $\Delta T_{\text{bubble}} / \langle \Delta T_{\text{bubble}} \rangle$  represents

508 the inverse of the ratio of the local and instantaneous gas concentration to the average gas hold-up.

509 Clearly, the measured probability density function differs from that of a random Poisson process

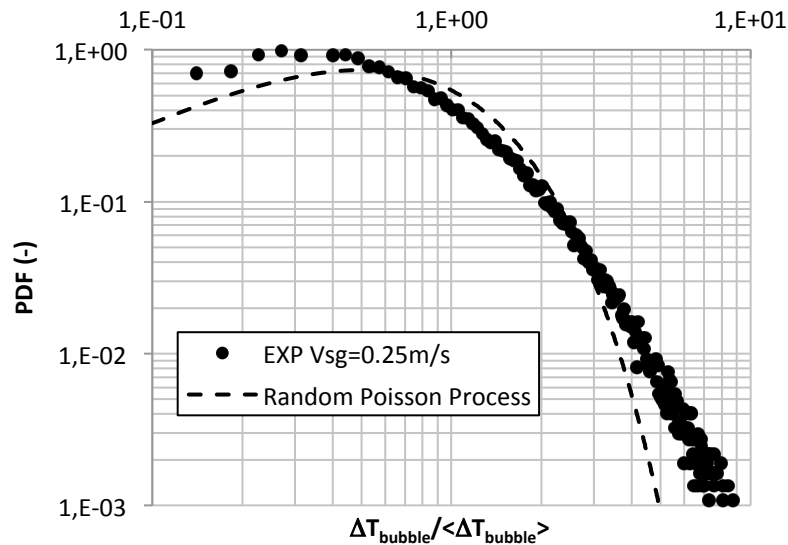
510 referred to as RPP in the sequel (Ferenc and Néda, 2007). In particular, the probability to found small

511 time intervals  $\Delta T_{\text{bubble}}$ , below  $0.6 \langle \Delta T_{\text{bubble}} \rangle$ , is higher than in RPP indicating that clusters (i.e. regions

512 where bubbles accumulate) are more probable than in a random process. Similarly, the probability to

513 found large time intervals  $\Delta T_{\text{bubble}}$ , above  $4 \langle \Delta T_{\text{bubble}} \rangle$ , is higher than in RPP indicating that voids (i.e.

514 regions with few bubbles) are also more probable than in RPP. This demonstrates that clusters and  
515 voids are indeed present in the heterogeneous regime (this behaviour holds for others columns size  
516 and superficial velocities). Moreover, that plot indicates that local, instantaneous concentrations  
517 evolve between 0.1 and 10 times the average gas holdup. Local, instantaneous concentrations  
518 varying over a so wide range imply quite strong fluctuations in density and thus in buoyancy.  
519 Therefore, one expects strong local velocity differences between dense and dilute regions. The latter  
520 can contribute to enhance the apparent relative velocity between phases as the bubbles are mostly  
521 located in clusters while the liquid is mostly present in voids. This may explain the large apparent  
522 relative velocity detected since the bubble terminal velocity in a still fluid is no longer the relevant  
523 scale. Such structures are also prone to contribute to turbulence production as they produce strong  
524 local and instantaneous shear rates. The velocity fluctuations shown in Figure 9 combined with the  
525 correlation (13) support that statement. Finally, if one sticks to the mean values of bubble sizes, the  
526 transition between homogeneous and heterogeneous regimes observed in the present experiments  
527 is not related with coalescence; instead, convective instabilities that lead to the formation of dense  
528 and dilute regions are believed to be responsible for that transition. To pursue along these lines, it  
529 would be worthwhile to characterise these clusters and voids in terms of gas holdup and size  
530 distributions and to examine how they evolve with flow conditions and column diameter. Another  
531 key issue is how to quantitatively relate these clusters and voids with the apparent relative motion  
532 between phases and with the turbulence production in the liquid phase. In particular it would be  
533 relevant to examine the connections between clusters and void dimensions and the correlation  
534 length scale  $\Lambda$  discussed above.



535

536 **Figure 11: Voronoi diagram deduced from an optical probe signal collected in the centre of the 1m diameter column**  
 537 **operated at Vsg =25cm/s (dots). The dashed line represents the statistics of a Random Poisson Process.**

538

## 539 5. Conclusions

540 The objective of this work was to study specifically the scale-up of bubble columns in the  
 541 heterogeneous regime using similar fluids and the same measurement techniques at very different  
 542 scales, which has never been reported before in literature. The wide range of column diameter, from  
 543 0.15 to 3m and of superficial gas velocities, from 0.05m/s to 0.35m/s, involved in this study makes  
 544 the reported data an important material for validation of Population Balance and CFD models and for  
 545 up-scaling issues. Correlations concerning gas holdup, mean liquid velocity and turbulence have been  
 546 validated over a wide range of geometry and operating conditions. In particular, the self-similarity of  
 547 the flow structure in terms of void fraction, liquid mean as well as fluctuating velocities have been  
 548 demonstrated in the heterogeneous regime. This is believed to hold while the aspect ratio of the  
 549 bubble column remains large enough so that end effects no longer affect the flow organisation in the  
 550 central portion of the column. That self-similarity leads to an entrained liquid flow rate proportional  
 551 to  $D^2(gD)^{1/2}$ , meaning that the entrainment capability of a bubble column is only set by its size and  
 552 does not depend on the injected gas superficial velocity. This result also demonstrates that the  
 553 velocity scale  $(gD)^{1/2}$  is a key descriptor for bubble column scale-up. Also, both the average and the

554 fluctuations of the liquid velocity are very sensitive to the scale-up. Small dependencies to the  
555 column diameter have been found on local and global gas holdup. The above results hold for all  
556 columns and flow conditions pertaining to the heterogeneous regime, and for almost the same  
557 average Sauter bubble diameters. The presence of strong concentration gradients has also been  
558 demonstrated, and the impact of these clusters and voids on the flow characteristics and on  
559 turbulence production deserves to be analysed further. As the turbulent dissipation rate plays an  
560 important role on the BSD, the turbulence induced in the heterogeneous regime needs to be better  
561 characterised in particular by determining its integral length scale.

562

### 563 **Abbreviations**

564	$d$	distance between probes (m or mm)
565	$d_{32}$	Local mean Sauter diameter (m or mm)
566	$\langle d_{32} \rangle$	volume averaged mean Sauter diameter (m or mm)
567	$d_{32,h}$	Local mean Sauter horizontal diameter (m or mm)
568	CC	cross-correlation
569	D	Column diameter (m)
570	$ecc$	bubble eccentricity
571	$H$	height from gas distributor (m)
572	$H_0$	static (non aerated) liquid height (m)
573	$H_D$	aerated liquid height (m)
574	$Q_G$	gas flow rate ( $m^3/s$ )
575	$Q_{G,core}$	gas flow rate in the core region( $m^3/s$ )
576	$Q_{L,up}$	Upward liquid flow rate in the core region ( $m^3/s$ )
577	$r$	Radial position (m)
578	R	radius of the column (m)
579	$S_c$	Section of the core region ( $m^2$ )

580  $U(x,t)$  Liquid axial instantaneous velocity (m/s)  
581  $U(x,t)$  Liquid axial average velocity (m/s)  
582  $U_0$  Liquid axial velocity at the center of the column (m/s)  
583  $U_r$  Relative velocity between gas and liquid (m/s)  
584  $u'$  RMS of liquid axial velocity fluctuation (m/s)  
585  $V_{sg}$  Superficial gas velocity (m/s)  
586  $x$  normalized radial position ( $=2r/D$ )

587 *Symbols*

588  $\alpha_G$  Local gas holdup  
589  $\langle\alpha_G\rangle$  Average gas holdup  
590  $\varepsilon$  Turbulence dissipation rate (w/kg)  
591  $\Lambda$  Turbulence macroscale (m)  
592  $\rho$  Liquid density ( $\text{kg/m}^3$ )

593

594 **References**

595 Besagni G., Di Pasquali A., Gallazzini L., Gottardi E., Colombo L. P. M. and Inzoli F. (2017a), The effect  
596 of aspect ratio in counter-current gas-liquid bubble columns: Experimental results and gas holdup  
597 correlations, *International Journal of Multiphase Flow*, 94, 53–78.  
598 Besagni, G., Inzoli, F. (2017b), The effect of liquid properties on bubble column fluid dynamics; gas  
599 hold-up, flow regime transition, bubble size distributions and shapes, interfacial areas and foaming  
600 phenomena, *Chem. Eng. Sci.*, 170, 270-296.  
601 Besagni, G., Inzoli, F., Ziegenheim, T. (2018), Two-Phase Bubble Columns: A Comprehensive Review,  
602 *ChemEngineering* 2(2), 13.  
603 Buffo, A., Vanni, M., Marchisio, D. L. and Fox, R. O. (2013), Multivariate quadrature-based moments  
604 methods for turbulent polydisperse gas-liquid system', *International Journal of Multiphase Flow* 50,  
605 41–57.

606 Chaumat, H., Billet-Duquenne, A.M., Augier, F., Mathieu, C., Delmas, H. (2005), Mass transfer in  
607 bubble column for industrial conditions—effects of organic medium, gas and liquid flow rates and  
608 column design, *Chemical Engineering Science*, Volume 60, Issue 22, 5930-5936.

609 Clift, R., Grace, J., Weber, M.E. (1978) *Bubbles, Drops, and Particles*, New York, NY : Dover Publ.

610 Deckwer, W., 1992. *Bubble Column Reactors*. Wiley, Chichester, New York.

611 Ferenc, F.S., Néda Z. (2007) On the size distribution of Poisson Voronoi cells. *Physica A: Statistical*  
612 *Mechanics and its Applications* 385(2), 518–526.

613 Forret, A., Schweitzer, J.M., Gauthier, T., Krishna, R. Schweich, D. (2003), Influence of scale on the  
614 hydrodynamics of bubble column reactors: an experimental study in columns of 0.1, 0.4 and 1m  
615 diameters. *Chemical Engineering Science*, Volume 58, Issues 3–6, 719-724.

616 Forret, A., Schweitzer, J.M., Gauthier, T., Krishna, R., Schweich, D. (2006), Scale Up of Slurry Bubble  
617 Reactors, *Oil & Gas Science and Technology - Rev. IFP*, Volume 61, Number 3, 443 – 458.

618 Gemello, L., Plais, C., Augier, F., Cloupet, A. and Marchisio, D. (2018a), Hydrodynamics and bubble  
619 size in bubble columns: Effects of contaminants and spargers, *Chemical Engineering Science* 184, 93–  
620 102.

621 Gemello, L., Cappello, V., Augier, F., Marchisio, D. and Plais, C. (2018b), CFD-based scale-up of  
622 hydrodynamics and mixing in bubble columns, *Chemical Engineering Research and Design*, 136, 846-  
623 858.

624 Guan X., Yang N., Li Z., Wang L., Cheng Y and Li X. (2016), Experimental Investigation of Flow  
625 Development in Large-Scale Bubble Columns in the Churn-Turbulent Regime, *Ind. Eng. Chem. Res.*,  
626 55, 3125–3130.

627 Guedon, G.R., Besagni G., Inzoli F. (2017), Prediction of gas-liquid flow in an annular gap bubble  
628 column using a bi-dispersed Eulerian model, *Chemical Engineering Science*, 161 , 138-150.

629 Jakobsen, H. A., Lindborg, H. and Dorao, C. A. (2005), Modeling of bubble column reactors: Progress  
630 and limitations, *Industrial & Engineering Chemistry Research* 44(14), 5107–5151.

631 Joshi, J. (2001), Computational flow modelling and design of bubble column reactors, Chemical  
632 Engineering Science 56(21), 5893–5933.

633 Kantarci, N., Borak, F., Ulgen, K.O., (2005), Bubble column reactors, Process Biochemistry 40 (2005)  
634 2263–2283.

635 Krishna R., Van Baten, J.M. (2001), Scaling up bubble column reactors with the aid of CFD, Trans  
636 IChemE, Vol. 79, Part A.

637 Lehr, F., Millies, M. and Mewes, D. (2004), Bubble-size distributions and flow fields in bubble  
638 columns, American Institute of Chemical Engineering Journal 48(11), 2426–2443.

639 Maximiano Raimundo, P. (2015), Analysis and modelization of local hydrodynamics in bubble  
640 columns, PhD thesis, Universit Grenoble Alpes, Grenoble, France.

641 Maximiano Raimundo, P., Cartellier, A., Beneventi, D., Forret, A. and Augier, F. (2016), A new  
642 technique for in-situ measurements of bubble characteristics in bubble columns operated in the  
643 heterogeneous regime, Chemical Engineering Science 155, 504 – 523.

644 McClure, D. D., Kavanagh, J. M., Fletcher, D. F. and Barton, G. W. (2013), Development of a CFD  
645 model of bubble column bioreactors: Part one a detailed experimental study, Chemical Engineering &  
646 Technology 36(12), 2065–2070.

647 McClure, D. D., Kavanagh, J. M., Fletcher, D. F. and Barton, G. W. (2014), Development of a CFD  
648 model of bubble column bioreactors: Part Two – Comparison of Experimental Data and CFD  
649 Predictions, Chemical Engineering & Technology 37(1), 131-140.

650 McClure, D. D., Norris, H., Kavanagh, J. M., Fletcher, D. F. and Barton, G. W. (2015), Towards a CFD  
651 model of bubble columns containing significant surfactant levels, Chemical Engineering Science 127,  
652 189–201.

653 McClure, D. D., Wang, C., Kavanagh, J. M., Fletcher, D. F. and Barton, G. W. (2016), Experimental  
654 investigation into the impact of sparger design on bubble columns at high superficial velocities,  
655 Chemical Engineering Research and Design 106, 205–213.

656 McClure, D. D., Kavanagh, J. M., Fletcher, D. F. and Barton, G. W. (2017), Experimental investigation  
657 into the drag volume fraction correction term for gas-liquid bubbly flows, *Chemical Engineering*  
658 *Science* 170, 91–97. 13th International Conference on Gas-Liquid and Gas-Liquid-Solid Reactor  
659 Engineering.

660 Menzel, T., In der Weide, T., Staudacher, O., Wein, O., Onken, U. (1990), Reynolds shear stress for  
661 modeling of bubble column reactors, *Ind. Eng. Chem. Res.*, 29 (6), pp 988–994.

662 Monchaux, R., Bourgoïn, M., Cartellier, A. (2012) Analyzing preferential concentration and clustering  
663 of inertial particles in turbulence. *International Journal of Multiphase Flow* 40, 1–18.

664 Miyauchi, T. and Shyu, C.N. (1970), Flow of fluid in gas bubble columns, *Kagaku Kogaku*, 34, 958-964.

665 Nottenkämper, R., Steiff, A. and Weinspach, P-M. (1983), Experimental investigation of  
666 hydrodynamics of bubble columns. *Ger. Chem. Eng.*, 6, 147-155.

667 Riemann J., Kusterer, H., John, H. (1983), Two-Phase flow rate measurements with pitot tubes and  
668 density measurements, In *Measuring Techniques in Gas-Liquid Two-Phase flows*, IUTAM Symposium  
669 Nancy, France, Ed. Delhaye J.M., Cagnet G., Publisher Springer Verlag.

670 Riquarts, H.P. (1981), A physical model for axial mixing of the liquid phase for heterogeneous flow  
671 regime in bubble columns. *German Chemical Engineering*, 4, 18-23.

672 Roels, J.A., Heijnen, J.J. (1980), Power dissipation and heat production in bubble columns: Approach  
673 based on nonequilibrium thermodynamics, *Biotechnology and Bioengineering*, Vol. XXII, 2399-2404.

674 Rollbusch, P., Bothe, M., Becker, M., Ludwig, M., Grünwald, M., Schlüter, M., Franke, R. (2015),  
675 Bubble columns operated under industrially relevant conditions - Current understanding of design  
676 parameters, *Chem. Eng. Sci.*, 126, 660–678.

677 Rusaouen, E., Riedinger, X., Tisserand, J.-C., Seychelles, F., Salort, J., Castaing, B. and Chillà, F. (2014)  
678 Laminar and intermittent flow in a tilted heat pipe, *Eur. Phys. J. E.* 37:4.

679 Ruzicka, M.C. (2013) On stability of a bubble column, *Chem. Eng. Research and Design* 91, 191-203

680 Sanya, J., Marchisio, D. L., Fox R. O., Dhanasekharan, K. (2005). On the Comparison between  
681 Population Balance Models for CFD Simulation of Bubble Columns, *Ind. Eng. Chem. Res.* 44, 14,  
682 5063-5072.

683 Sasaki S., Hayashi K., Tomiyama A. (2016). Effects of liquid height on gas holdup in air–water bubble  
684 column, *Exp. Therm. Fluid Sc.* 72, 67–74.

685 Schweitzer, J.-M. (2001). Local gas hold-up measurements in fluidized bed and slurry bubble column.  
686 *Chem. Eng. Sci.* 56 (3), 1103–1110.

687 Tisserand, J.-C., Creyssels, M., Gibert, M., Castaing, B. and Chillà, F. (2010) Convection in a vertical  
688 channel, *New Journal of Physics* 12, 075024.

689 Xue, J. (2004), Bubble velocity, size and interfacial area measurements in bubble columns, PhD thesis,  
690 Sever Institute of Washington University, St. Louis, Missouri.

691 Xue, J., Al-Dahhan, M., Dudukovic, M.P. and Mudde, R.F. (2008) Bubble Velocity, size, interfacial area  
692 measurements in a bubble column by four-point optical probes, *AIChE J.*, 54(2), 350-363.

693 Zehner, P. (1986), Momentum, mass and heat transfer in bubble columns, Part 1 Flow model of the  
694 bubble column and liquid velocities. *Int. Chem. Eng.*, 41, 1969-1977.

695 Zuber, N., Findlay, J.A. (1965), Average Volumetric Concentration in Two-Phase Flow Systems, *J. Heat*  
696 *Transfer.*, 87,4, 453-468

697

698

699 *Acknowledgements*

700 LEGI and LGP2 laboratories are part of the LabEx Tec 21 (Investissements d’Avenir-Grant Agreement

701 No. ANR-11-LABX-0030).